Intermetallics 123 (2020) 106837

Contents lists available at ScienceDirect

Intermetallics

journal homepage: http://www.elsevier.com/locate/intermet

Crystal structure and complex magnetic properties of $R_{11}Pd_4In_9$ compounds (R = Y, Gd–Er)

S. Baran [a,*], Yu. Tyvanchuk [b], B. Penc [a], Ya. Kalychak [b], A. Hoser [c], A. Szytuła [a]

[a] M. Smoluchowski Institute of Physics, Jagiellonian University, Łojasiewicza 11, 30-348, Kraków, Poland
[b] Analytical Chemistry Department, Ivan Franko National University of Lviv, Kyryla i Mefodiya 6, 79005, Lviv, Ukraine
[c] Helmholtz-Zentrum Berlin für Materialien und Energie GmbH, Hahn-Meitner Platz 1, D-14109, Berlin, Germany

ARTICLE INFO

Keywords:
Intermetallics
Magnetically ordered materials
Crystal structure
Magnetic measurements
Magnetic structure
Neutron diffraction

ABSTRACT

Magnetic properties of the $R_{11}Pd_4In_9$ compounds (R = Y, Gd–Er) were investigated by means of X-ray diffraction and magnetic measurements. Three of these compounds, namely those with R = Y, Ho and Er, are newly synthesized. The compounds crystallize in the orthorhombic $Nd_{11}Pd_4In_9$-type crystal structure (oC48, *Cmmm*) in which the rare earth atoms occupy five nonequivalent sublattices. Magnetic properties of the investigated compounds are related mainly to the R^{3+} ions, except the case of $Y_{11}Pd_4In_9$ which is a Pauli paramagnet. For R = Gd-Er, the values of effective magnetic moments in the paramagnetic state are close to the free R^{3+} ion values while the moments in the ordered state at $T = 2$ K and $H = 90$ kOe are lower than the respective R^{3+} moments. The compounds have complex magnetic properties. All paramagnetic Curie temperatures are positive suggesting that the ferromagnetic interactions are predominant. However, the low temperature data indicate an antiferromagnetic order. With increase of temperature the magnetic properties change from antiferro-to ferrimagnetic and finally to paramagnetic ones. The critical temperatures of magnetic ordering do not fulfill the de Gennes scaling, indicating a crystalline electric field contribution to stabilization of the magnetic order at low temperatures. The neutron diffraction measurements, performed for $Ho_{11}Pd_4In_9$, reveal a coexistence of two magnetic phases at low temperatures: the antiferromagnetic with propagation vector $\boldsymbol{k}$ = [0,0,½] and the ferrimagnetic one with $\boldsymbol{k}$ = [0,0,0]. The antiferromagnetic order is predominant at low temperatures while the ferrimagnetic one dominates at intermediate temperatures.

1. Introduction

The rare-earth—transition metal—In (R-T-In) ternary systems form a rich group of the intermetallic compounds with interesting crystal structure and unique physical properties [1]. In recent years the isostructural $R_{11}Ni_4In_9$ compounds ($Nd_{11}Pd_4In_9$-type structure, Pearson symbol oC48, space group *Cmmm*) were intensively investigated. According to magnetic measurements they exhibit complex magnetic properties at low temperatures with multiple magnetic transitions [2–6]. Investigation of the fibrous samples of $R_{11}Ni_4In_9$ (R = Gd, Tb, Dy and Ho) revealed strong magnetic anisotropy with easy magnetization along the *c*-axis [4–6]. Neutron diffraction data for $R_{11}Ni_4In_9$ (R = Tb and Ho) showed that magnetic moments in different sublattices order at different temperatures [6].

During investigation of the R-Pd-In system at 870 K an existence of the $R_{11}Pd_4In_9$ (R = La, Ce, Pr, Nd, Sm, Gd, Tb, Dy) compounds [7] with the $Nd_{11}Pd_4In_9$-type structure [8] has been established. The compounds have complex crystal structure in which the rare earth atoms occupy five nonequivalent crystallographic positions.

Among the $R_{11}Pd_4In_9$ compounds, their magnetic properties have already been determined only for $Ce_{11}Pd_4In_9$, which is a ferromagnet below $T_c = 18.6$ K with additional order-order magnetic transition at $T_t = 1.6$ K [9].

This work is a part of our investigation of magnetic properties of ternary rare-earth—transition metal indides, in purpose to determine the influence of different factors, like: composition, crystal structure and chemical bonding, on magnetic properties of these compounds. In the previous work we have concentrated on the compounds with T = Ni [2,3,10]. In this work we report the results of X-ray diffraction and dc magnetic measurements of the $R_{11}Pd_4In_9$ (R = Y, Gd–Er) compounds. From these data, the crystal structure parameters at room temperature as well as magnetic properties within the temperature range between 1.9

* Corresponding author.
E-mail address: stanislaw.baran@uj.edu.pl (S. Baran).

https://doi.org/10.1016/j.intermet.2020.106837
Received 31 March 2020; Received in revised form 8 May 2020; Accepted 10 May 2020
Available online 19 May 2020

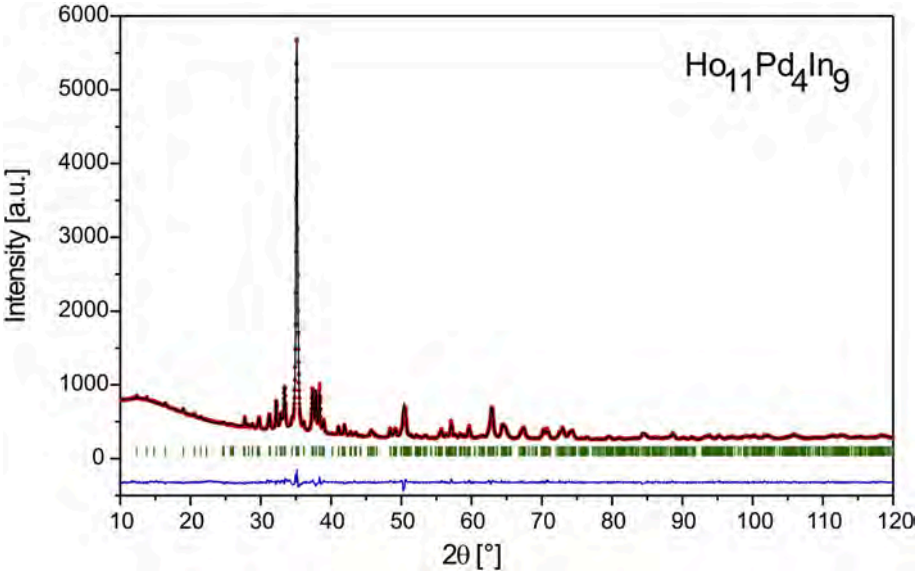

Fig. 1. X-ray diffraction pattern (CuK_α – radiation) of $Ho_{11}Pd_4In_9$ collected at room temperature. The solid circles are for the experimental data, the line shows the result of Rietveld refinement, the vertical bars mark the Bragg reflection positions while the difference between the experimental data and the refinement is plotted at the bottom of the figure.

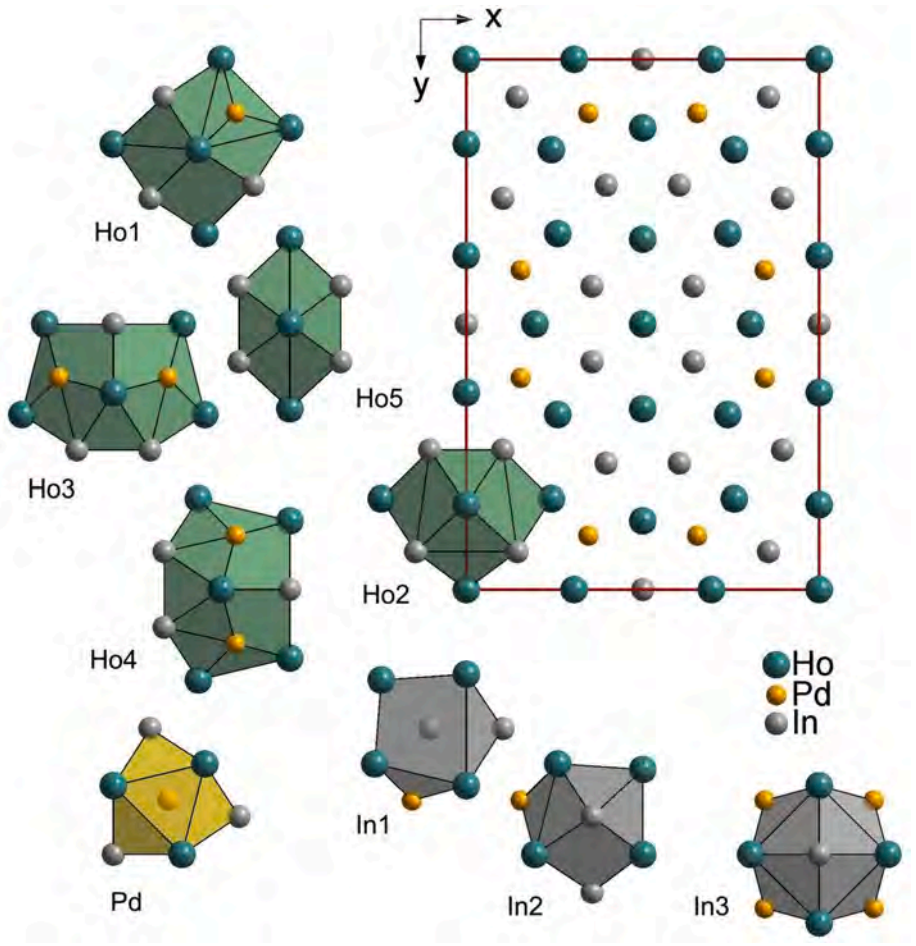

Fig. 2. Projection of the $Ho_{11}Pd_4In_9$ crystal structure onto the *xy* plane and coordination polyhedra of atoms.

Table 1
Crystallographic data obtained from Rietveld refinement, based on the X-ray powder diffraction patterns collected at room temperature for $R_{11}Pd_4In_9$ ($Nd_{11}Pd_4In_9$–type structure, space group *Cmmm*).

R	Y	Gd	Tb	Dy	Ho	Er
M [g/mole]	2437.01	3188.79	3207.22	3246.54	3273.27	3298.89
a [Å]	14.515(3)	14.606(2)	14.540(2)	14.489(3)	14.450(2)	14.420(2)
b [Å]	21.853(3)	21.985(3)	21.872(3)	21.802(4)	21.743(3)	21.710(3)
c [Å]	3.6535(6)	3.6997(9)	3.6737(9)	3.6455(10)	3.6326(4)	3.6138(4)
V [Å^3]	1158.9(5)	1188.1(4)	1168.3(3)	1151.6(5)	1141.3(2)	1131.6(3)
*R*1 at 8*p* (*x*, *y*, 0)	$x = 0.240(1)$	0.2387(7)	0.2390(7)	0.240(1)	0.2408(8)	0.241(2)
	$y = 0.174(1)$	0.1726(5)	0.1726(5)	0.171(1)	0.1708(4)	0.172(1)
*R*2 at 4*i* (0, *y*, 0)	$y = 0.161(2)$	0.1603(7)	0.1602(7)	0.160(1)	0.1601(8)	0.158(2)
*R*3 at 4*i* (0, *y*, 0)	$y = 0.372(1)$	0.3730(7)	0.3722(7)	0.371(1)	0.3705(8)	0.372(2)
*R*4 at 4*g* (*x*, 0, 0)	$x = 0.303(2)$	0.3098(11)	0.3080(10)	0.308(2)	0.3056(12)	0.301(2)
*R*5 at 2*a* (0, 0, 0)						
Pd at 8*q* (*x*, *y*, ½)	$x = 0.345(1)$	0.3441(9)	0.3454(9)	0.344(2)	0.3458(8)	0.344(2)
	$y = 0.102(1)$	0.0987(7)	0.0996(7)	0.101(1)	0.1017(8)	0.102(2)
In1 at 8*q* (*x*, *y*, ½)	$x = 0.105(1)$	0.1027(7)	0.1029(7)	0.103(1)	0.1037(8)	0.106(2)
	$y = 0.263(1)$	0.2619(5)	0.2610(5)	0.261(1)	0.2624(8)	0.262(2)
In2 at 8*q* (*x*, *y*, ½)	$x = 0.144(1)$	0.1460(9)	0.1447(9)	0.144(2)	0.1438(8)	0.146(3)
	$y = 0.072(1)$	0.0731(5)	0.0733(5)	0.073(1)	0.0715(4)	0.071(2)
In3 at 2*c* (½, 0, ½)						
$B_{over.}$ [Å^2]	1.2(2)	1.2(2)	1.4(2)	0.9(3)	1.9(2)	1.8(1)
G1 texture parameter[a] [001]	0.09(3)	0.90(2)	0.88(2)	0.55(3)	0.28(2)	0.04(3)
R_F [%]	3.08	3.78	3.76	5.32	2.71	6.24
R_{Bragg} [%]	5.43	7.79	6.81	6.35	4.42	6.61

[a] The G1 parameter of the original Rietveld preferred orientation function (NOR = 0).

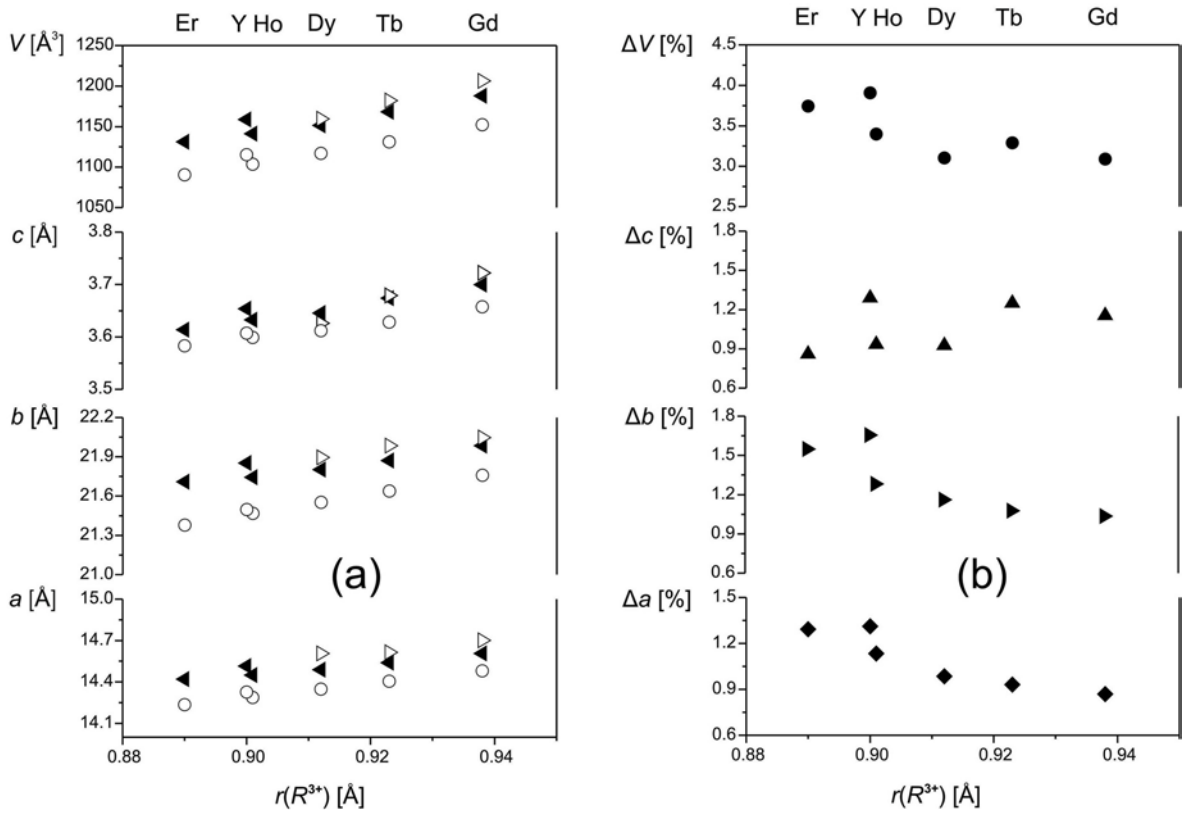

Fig. 3. (a) Lattice parameters *a*, *b* and *c* along with the unit cell volume *V* for the $R_{11}T_4In_9$ (T = Ni, Pd) compounds as a function of $r(R^{3+})$ - the effective ionic radius of heavy rare-earths with coordination number VI. The filled triangle symbols refer to the experimental data for $R_{11}Pd_4In_9$ as presented in this work while the open ones - to the literature data from Ref. [7]. The open circles refer to the $R_{11}Ni_4In_9$ series accordingly to the literature data from Refs. [2,3,5,10]. (b) Relative changes in the lattice parameters of $R_{11}T_4In_9$ (T = Ni, Pd) as a function of $r(R^{3+})$. $\Delta a = [(a(Pd)\text{-}a(Ni))/a(Ni)] \times 100\%$, etc. The radii were taken from Ref. [12].

and 390 K and external magnetic fields (up to 90 kOe) are determined.

In order to explain the complex magnetic properties of $Ho_{11}Pd_4In_9$, additional neutron diffraction measurements at low temperatures were performed.

2. Experiment

The samples of $R_{11}Pd_4In_9$ were prepared by arc-melting of high purity metals (99.9 wt% purity for R, 99.99 wt% for Pd and In) having total mass of 1.5 g under a pure argon atmosphere. The buttons were sealed in evacuated silica tubes and annealed at 870 K for one month. The

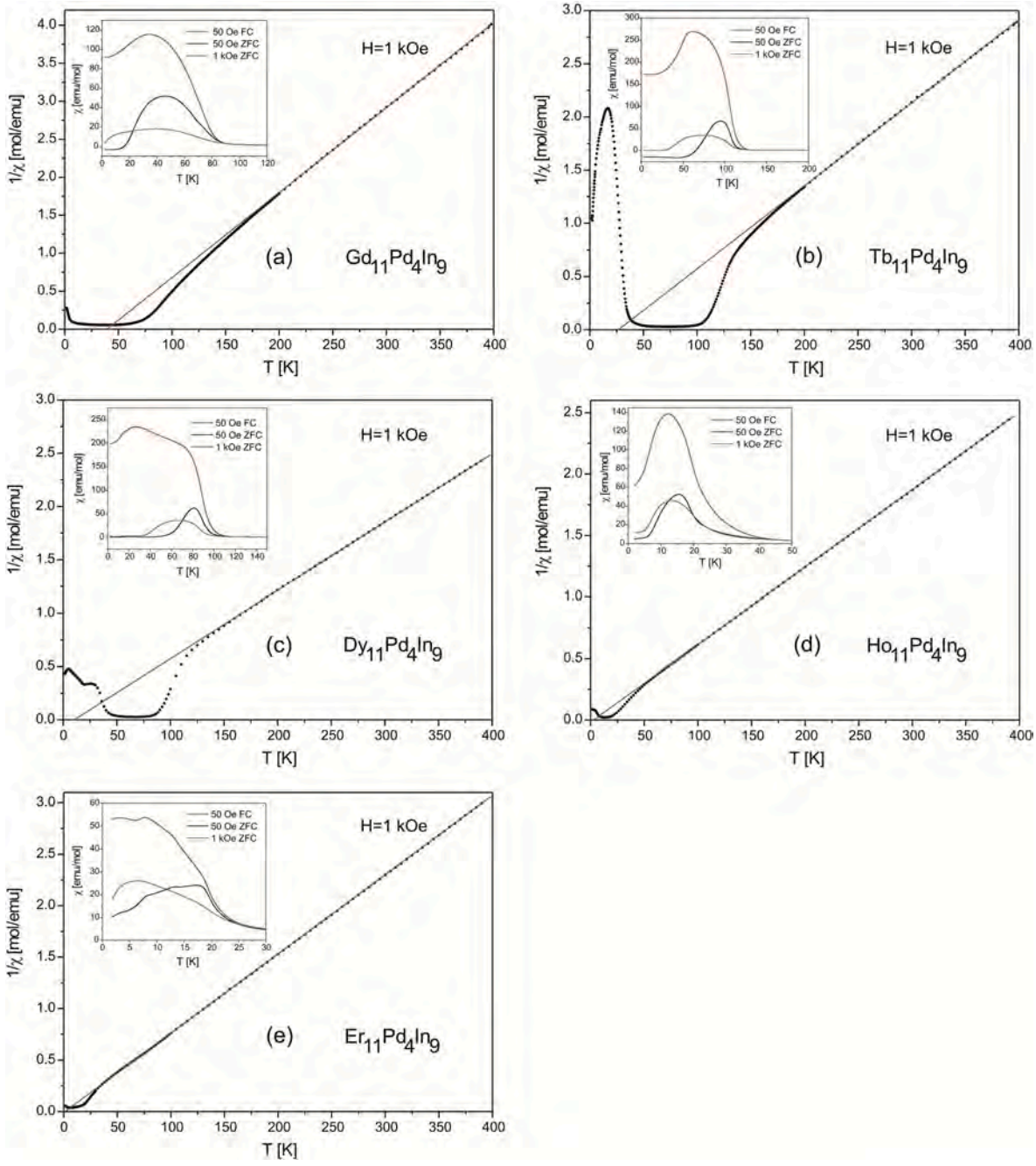

Fig. 4. Reciprocal magnetic susceptibility (circles) together with fitted line representing the Curie-Weiss law for $R_{11}Pd_4In_9$: (a) R = Gd, (b) Tb, (c) Dy, (d) Ho and (e) Er. The upper insets show the low temperature behavior measured at 50 Oe (ZFC and FC) and 1 kOe (ZFC).

Table 2
Magnetic properties of $R_{11}Pd_4In_9$ (R = Gd–Er): the Curie and transitions temperature (T_c, T_t), the paramagnetic Curie temperature (θ_p), experimental (exp.) and theoretical (theor.) values of the effective magnetic moment (μ_{eff}) and of the moment in the ordered state (μ) at T = 1.9 K (or 2.0 K for $Tb_{11}Pd_4In_9$) and H = 90 kOe together with the theoretical value for free R^{3+} ion.

R	T_c [K]	T_t [K]	θ_p [K]	μ_{eff} [μ_B]		μ [μ_B]	
				exp.	theor.	exp.	theor.
Gd	66	23	37	8.09	7.94	2.48	7.0
Tb	106	78	24	9.70	9.72	2.20	9.0
Dy	88	70	11.2	10.64	10.65	4.14	10.0
Ho	18.7	8.4	3.0	10.73	10.61	6.89	10.0
Er	19.6	7.0	1.1	9.72	9.59	5.48	9.0

powdered polycrystalline samples were measured at room temperature using a PANalytical X'Pert PRO diffractometer (Cu K_α -radiation, Bragg-Brentano geometry, measured angle interval 2θ = 10-130°, step scan mode, step size in 2θ = 0.026°, 480 s/step). The FullProf [11] program package was used for X-ray phase and Rietveld analysis of the collected data set.

The magnetic measurements were carried out using a vibrating sample magnetometer (VSM) option of the Quantum Design PPMS platform. Three types of magnetic measurements were performed: collecting ZFC (zero field cooling) and FC (field cooling) magnetic susceptibility curves in applied field of H = 50 Oe from 1.9 to 390 K (in order to determine phase transition temperatures), then scanning from 1.9 K up to 390 K in magnetic field of 1 kOe (in order to determine the effective magnetic moment μ_{eff} and paramagnetic Curie temperature θ_p)

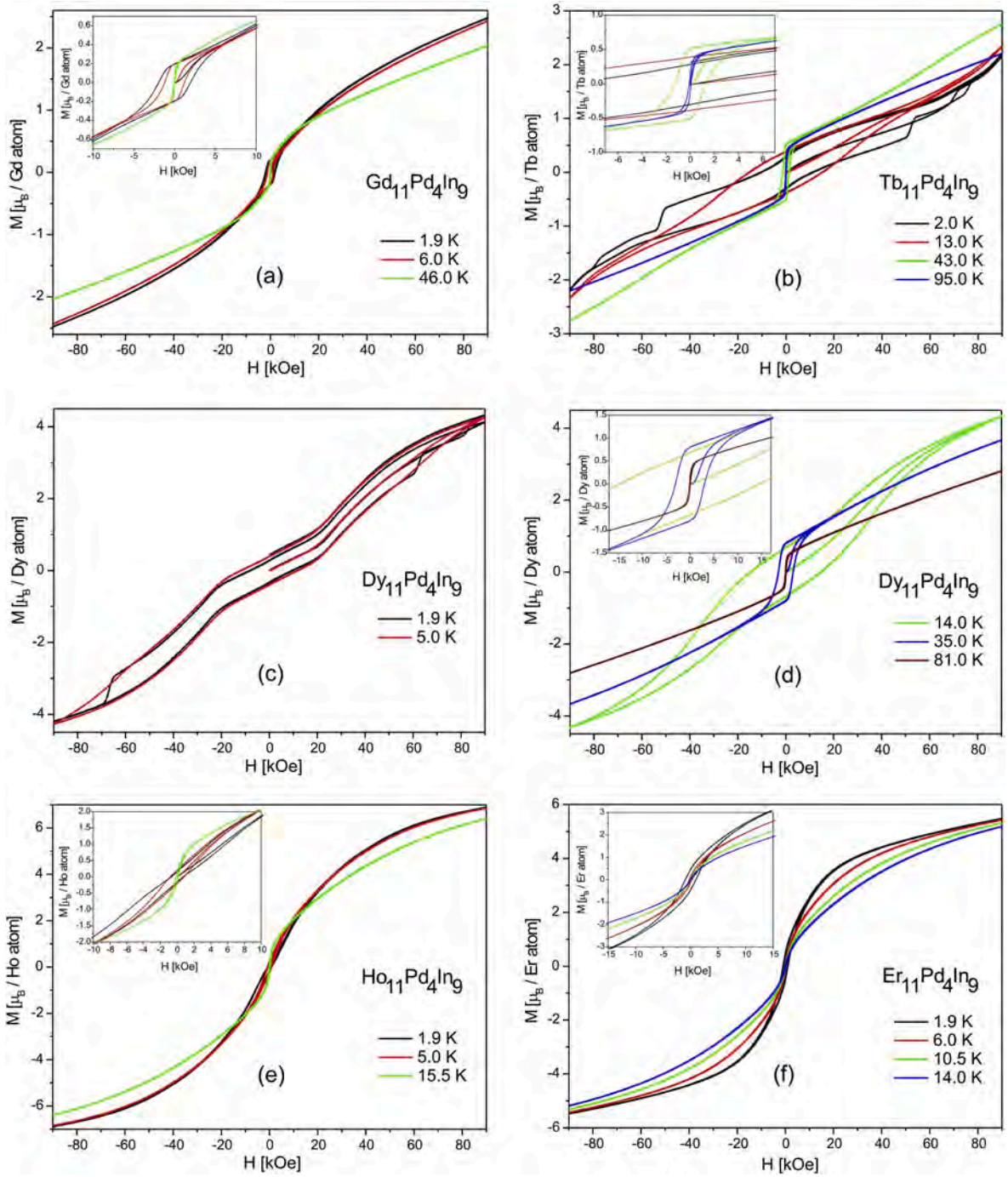

Fig. 5. Isothermal magnetization of $R_{11}Pd_4In_9$ compounds vs. external magnetic field at selected temperatures for (a) R = Gd, (b) Tb, (c, d) Dy, (e) Ho and (f) Er. The insets show magnetization at low magnetic fields.

and finally measuring magnetization curves and hysteresis loops up to 90 kOe at selected temperatures.

For the polycrystalline sample of $Ho_{11}Pd_4In_9$ additional powder neutron diffraction measurements with the use of the E6 diffractometer installed at the BERII reactor (BENSC, Helmholtz-Zentrum Berlin) were performed. The incident neutron wavelength was $\lambda = 2.432$ Å while temperature ranged from 1.5 up to 24.6 K The Rietveld-type program FullProf [11] was used for processing the data.

3. Results

3.1. Crystal structure

X-ray powder diffraction data collected at room temperature for the $R_{11}Pd_4In_9$ samples indicate (Fig. 1 shows exemplary data for $Ho_{11}Pd_4In_9$) that the investigated compounds crystallize in the $Nd_{11}Pd_4In_9$-type crystal structure (Pearson symbol oC48, space group *Cmmm*) [8]. Fig. 2 shows the projection of the atoms on the *xy* plane for $Ho_{11}Pd_4In_9$ and illustrates the coordination polyhedra of all the atoms, viz. $[Ho1Pd_2In_6Ho_6]$, $[Ho2In_8Ho_5]$, $[Ho3Pd_4In_6Ho_6]$, $[Ho4Pd_4In_6Ho_6]$, $[Ho5In_8Ho_4]$, $[PdHo_6In_3]$, $[In1In_3PdHo_8]$, $[In2PdIn_3Ho_8]$,

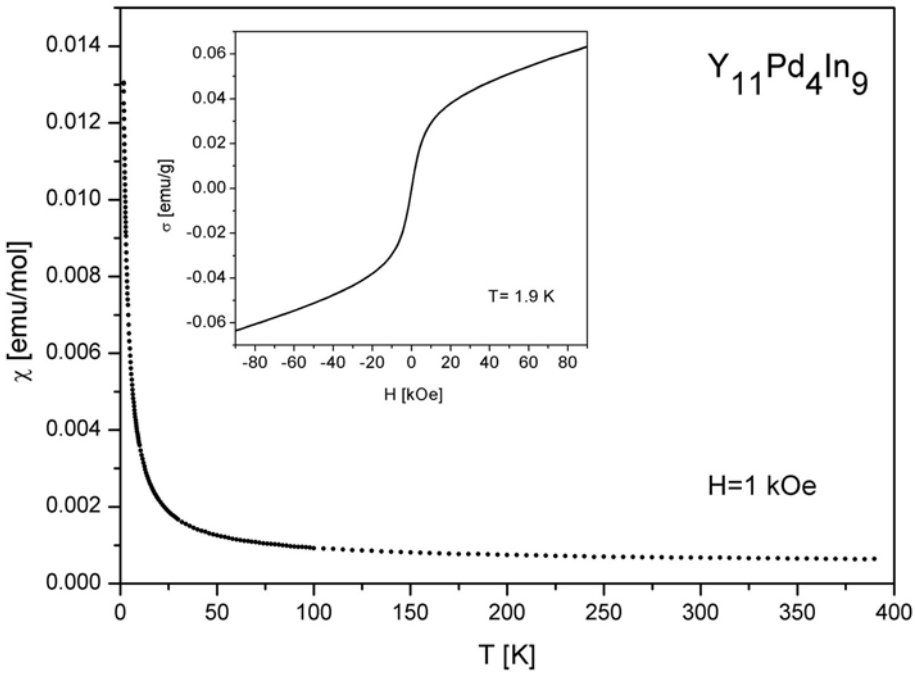

Fig. 6. Temperature dependence of the $Y_{11}Pd_4In_9$ magnetic susceptibility taken at H = 1 kOe. The inset shows the magnetization curve at T = 1.9 K.

Table 3
The critical fields for metamagnetic transitions (H_{cr}) and coercivity fields (H_{co}) in $R_{11}Pd_4In_9$ (R = Gd–Er) as determined from magnetization vs. applied magnetic field curves. The values in brackets indicate temperatures of measurements.

R	H_{cr} [kOe]	H_{co} [kOe]
Gd	1.75 (1.9 K), 0.65 (6.0 K), 0.03 (46.0 K)	1.95 (1.9 K), 1.20 (6.0 K), 0.04 (46.0 K)
Tb	70 (2.0 K), 25 (13.0 K), 0.7 (43.0 K), 0.06 (95.0 K)	10.3 (2.0 K), 15.2 (13.0 K), 1.30 (43.0 K), 0.07 (95.0 K)
Dy	27 (1.9 K and 5.0 K), 34 (14.0 K), 2.3 (35.0 K), 0.07 (81.0 K)	8.0 (1.9 K), 11.8 (5.0 K), 14.8 (14.0 K), 3.1 (35.0 K), 0.10 (81.0 K)
Ho	5.6 (1.9 K), 1.90 (5.0 K), 0.20 (15.5 K)	0.72 (1.9 K), 0.82 (5.0 K), 0.13 (15.5 K)
Er	1.70 (1.9 K), 0.45 (6.0 K), 0.22 (10.5 K), 0.12 (14.0 K)	0.96 (1.9 K), 0.23 (6.0 K), 0.10 (10.5 K), 0.05 (14.0 K)

[$In3Pd_4Ho_8In_2$]. The Ho atoms, which are situated at five different Wyckoff positions, occupy one layer of the structure ($z = 0$) while the second one ($z = ½$) is occupied by the palladium and indium atoms. Refined lattice parameters and atomic coordinates are presented in Table 1 and they are in good agreement with the previous results reported in Ref. [7]. The dependence of the lattice parameters *a, b* and *c* and the unit cell volume *V* (Fig. 3a) vs. effective ionic radius [12] is almost linear and agrees with the lanthanide contraction. The novel $R_{11}Pd_4In_9$ compounds with R = Y, Ho and Er prolong the concerned series.

3.2. Magnetic data

3.2.1. dc magnetic susceptibility

The results of magnetic measurements for the $R_{11}Pd_4In_9$ compounds (R = Gd–Er) are presented in Fig. 4a–e and 5a-5f and summarized in Table 2. At high temperatures the reciprocal magnetic susceptibilities of all compounds obey the Curie-Weiss law. The paramagnetic Curie temperatures, as determined from these data, are positive, while the values of effective magnetic moments are close to those predicted for the free R^{3+} ions (see Table 2).

With decrease of temperature a sharp increase of magnetic susceptibility is observed at 66, 106, 88, 18.7 and 19.6 K for R = Gd, Tb, Dy, Ho and Er, respectively (see upper insets in Fig. 4a–e). The above temperatures have been determined from inflection points in the ZFC χ(T) curves taken at 50 Oe and are listed in Table 2 as corresponding Curie points. Below Curie temperatures large discrepancies between the ZFC and FC curves are observed. Both curves show additional anomalies at lower temperatures, namely, the maxima at 46 K (ZFC) and 34 K (FC) for R = Gd, 95 K (ZFC) and 62 K (FC) for R = Tb, 81 K (ZFC) and 26 K (FC) for R = Dy, 15.4 K (ZFC) and 12.3 K (FC) for R = Ho and 17.3 K (ZFC) and 7.9 K (FC) for R = Er are observed. Further decrease of temperature leads to rapid decrease of susceptibility indicating additional magnetic transition of the order-order type. The corresponding transition temperatures determined from inflection points in the ZFC χ(T) curves are listed in Table 2.

Deviations from the Curie-Weiss law are observed below 250 K (R = Gd and Tb), 170 K (R = Dy), 60 K (R = Ho) and 40 K (R = Er) indicating existence of short-range magnetic order above corresponding Curie temperatures.

Magnetic susceptibility of $Y_{11}Pd_4In_9$ (Fig. 6) takes small values (<0.001 emu/mol) over broad temperature range suggesting that $Y_{11}Pd_4In_9$ is a Pauli paramagnet. This result is in agreement with small magnetic moment ($2.5 \cdot 10^{-3}$ μ_B/Y atom) determined from magnetization measured at 1.9 K. The increase of susceptibility below 100 K is probably related to small amount of magnetic atoms present as impurity in yttrium which is of 99.9 wt% purity.

3.2.2. Magnetization

Magnetization curves and hysteresis loops for $R_{11}Pd_4In_9$ (R = Gd–Er), measured at selected temperatures in external magnetic fields up to 90 kOe (9 T), are presented in Fig. 5a–f with insets showing the low-field range. The data indicate an influence of external magnetic field on the magnetic ground state. The primary curves, taken for the Gd-compound, indicate metamagnetic phase transitions with the critical fields equal to 1.75 kOe (1.9 K), 0.65 kOe (6.0 K) and 0.03 kOe (46.0 K). The above fields have been determined from inflection points in the primary M(H) curves. The hysteresis loops are characterized by the coercivity fields of 1.95, 1.20 and 0.04 kOe for 1.9, 6.0 and 46.0 K, respectively. The magnetization curve and hysteresis loop, measured at 46.0 K, are typical of a soft ferrimagnetic material. The magnetization

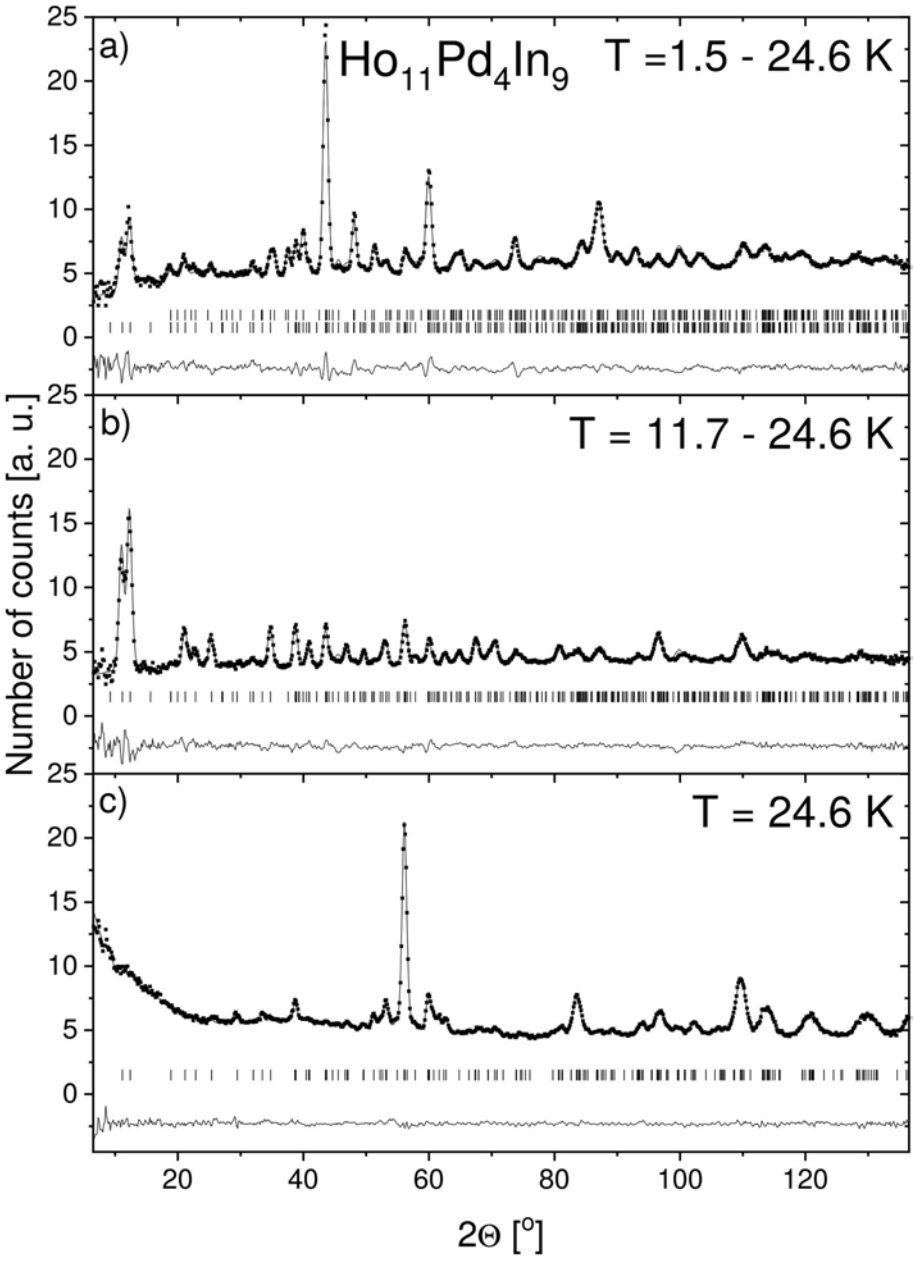

Fig. 7. Neutron diffraction patterns of $Ho_{11}Pd_4In_9$: the difference patterns of (a) (1.5–24.6 K) and (b) (11.7–24.6 K) together with (c) the pattern collected at 24.6 K. The squares represent the experimental points, the solid lines are for the calculated profiles for the crystal and magnetic structure models (as described in the text) and for the difference between the observed and calculated intensities (in the bottom of each diagram). The vertical bars indicate the positions of Bragg reflections related to: (a) AFM (the upper row) and FiM (the bottom row) magnetic phases, (b) FiM phase and (c) crystal structure.

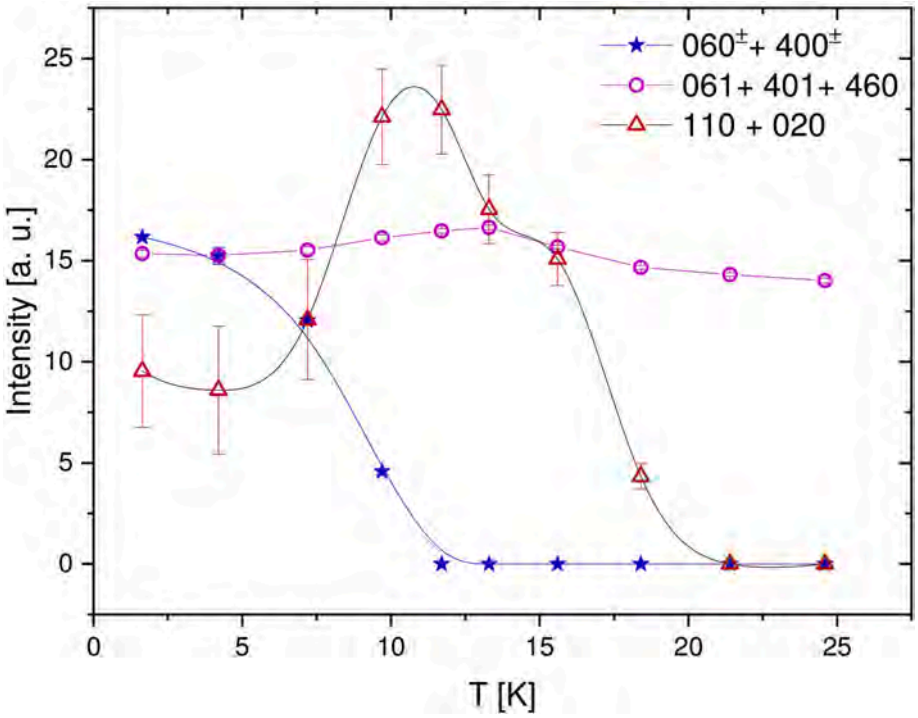

Fig. 8. Temperature dependence of Bragg reflection intensities related to the antiferromagnetic (AFM) phase (stars), ferrimagnetic (FiM) phase (triangles) and crystal structure (circles). Due to reflection overlapping the sums of selected reflections are shown as indicated in the legend.

curves do not show saturation at the highest field available, i.e. 90 kOe (9 T). The value of magnetic moment at T = 1.9 K and H = 90 kOe equals 2.48 μ_B/Gd atom.

The primary magnetization curve taken at 2.0 K for $Tb_{11}Pd_4In_9$ shows a metamagnetic phase transition in form of a jump at 70 kOe while the curves collected at higher temperatures show metamagnetic phase transitions at 25 kOe (13.0 K), 0.7 kOe (43.0 K) and 0.06 kOe (95.0 K). Hysteresis loops with the coercivity fields equal to 10.3 kOe (2.0 K), 15.2 kOe (13.0 K), 1.30 kOe (43.0 K), 0.07 kOe (95.0 K) are observed. The magnetic moment at T = 2.0 K and H = 90 kOe equals 2.20 μ_B/Tb atom while the moment at T = 43.0 K and H = 90 kOe reaches 2.76 μ_B/Tb atom.

The primary magnetization curves of $Dy_{11}Pd_4In_9$, collected at selected temperatures, indicate several metamagnetic transitions, namely, at 27 kOe (1.9 K and 5.0 K), 34 kOe (14.0 K), 2.3 kOe (35.0 K) and 0.07 kOe (81.0 K). The coercivity fields equal 8.0 kOe (1.9 K), 11.8 kOe (5.0 K), 14.8 kOe (14.0 K), 3.1 kOe (35.0 K) and 0.10 kOe (81.0 K). The magnetic moment at T = 1.9 K and H = 90 kOe equals 4.14 μ_B/Dy atom. Similar value of 4.32 μ_B/Dy atom is found at T = 14.0 K and H = 90 kOe.

It is worth noting that hysteresis loops collected at the lowest temperatures for $R_{11}Pd_4In_9$ (R = Tb and Dy) show a number of jumps indicating field-induced switching between metastable magnetic orderings.

Different shape of magnetization vs. external magnetic field curves is observed in $R_{11}Pd_4In_9$ (R = Ho, Er). In the ordered state, regardless the temperature, these dependences are similar to those observed for ferrimagnetic materials. The critical fields of metamagnetic transitions are low, namely, they equal to 5.6 kOe (1.9 K), 1.90 kOe (5.0 K), 0.20 kOe (15.5 K) in $Ho_{11}Pd_4In_9$ and 1.70 kOe (1.9 K), 0.45 kOe (6.0 K), 0.22 kOe (10.5 K), 0.12 kOe (14.0 K) in $Er_{11}Pd_4In_9$. Also the coercivity fields are low: 0.72 kOe (1.9 K), 0.82 kOe (5.0 K), 0.13 kOe (15.5 K) in $Ho_{11}Pd_4In_9$ and 0.96 kOe (1.9 K), 0.23 kOe (6.0 K), 0.10 kOe (10.5 K), 0.05 kOe (14.0 K) in $Er_{11}Pd_4In_9$. The magnetic moments at T = 1.9 K and H = 90 kOe equal 6.89 μ_B per Ho atom and 5.48 μ_B per Er atom.

Table 4
Ho magnetic moments as refined from the neutron diffraction pattern of $Ho_{11}Pd_4In_9$ collected at 1.5 K together with corresponding reliability factors. The AFM and FiM denote the antiferro- and ferrimagnetic contributions to the magnetic structure, respectively.

Site	μ_{AFM} [μ_B] (k = [0,0,½])	μ_{FiM} [μ_B] (k = [0,0,0])
Ho1	4.4(1)	2.9(2)
Ho2	4.7(1)	4.5(2)
Ho3	5.4(1)	−0.8(2)
Ho4	5.5(1)	−2.2(2)
Ho5	4.6(1)	0
R_{magn} [%]	9.1	18.8

It is worth noting that none of the magnetization curves shows saturation at 90 kOe and the determined magnetic moments per rare earth atoms are smaller than the theoretical values expected for free R^{3+} ions, even at the lowest temperatures.

The values of critical and coercivity fields, as determined from the magnetization vs. applied magnetic field dependences, are summarized in Table 3.

3.3. Neutron diffraction data

The results of powder neutron diffraction data for $Ho_{11}Pd_4In_9$, collected at three selected temperatures (1.5, 11.7 and 24.6 K), are presented in Fig. 7. Analysis of the paramagnetic pattern taken at T = 24.6 K confirms the crystal structure of the $Nd_{11}Pd_4In_9$-type (R_{Bragg} = 6.51%, R_F = 4.71%). Additional Bragg reflections of magnetic origin are

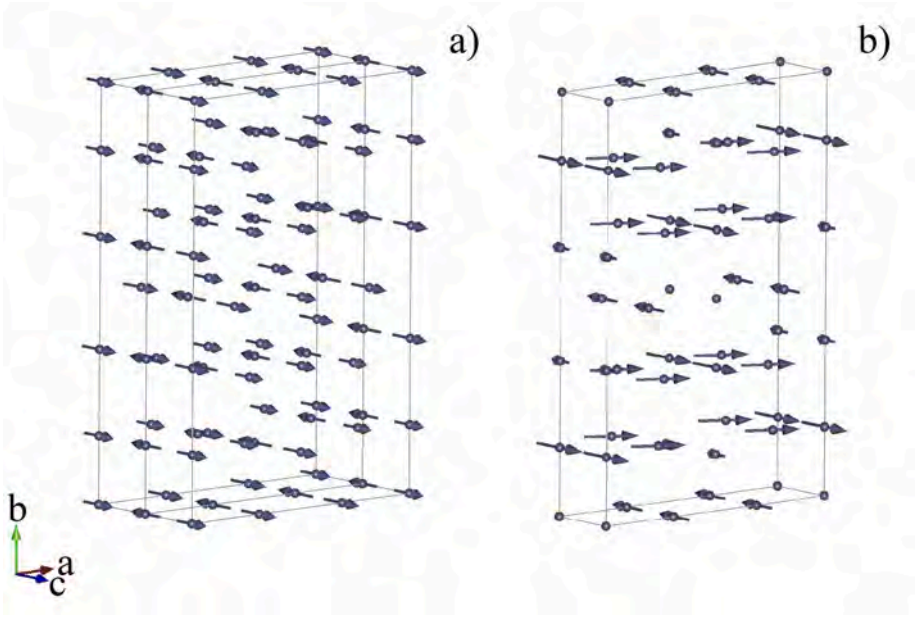

Fig. 9. The (a) antiferro- (AFM) and (b) ferrimagnetic (FiM) contributions to the magnetic structure of $Ho_{11}Pd_4In_9$.

visible in the patterns collected at 1.5 and 11.7 K. These reflections can be divided into two groups: the one related to the propagation vector $\boldsymbol{k}$ = [0,0,½] and the second one related to $\boldsymbol{k}$ = [0,0,0].

Analysis of the diffraction pattern at 1.5 K shows that the most intense reflections correspond to the antiferromagnetic structure with magnetic unit cell doubled along the *c*-axis when compared to the crystallographic one ($\boldsymbol{k}$ = [0,0,½]). The best fit has been obtained for a magnetic structure with all holmium magnetic moments within the crystallographic unit cell coupled ferromagnetically and parallel to the *c*-axis direction while the moments in the neighbouring cells along the *c*-axis point at opposite direction (see Fig. 9a). The exact values of magnetic moments are listed in Table 4, where Ho1, …, Ho5 refer to atoms located at different Wyckoff sites as specified in Table 1. The holmium moments are significantly smaller than 10 μ_B expected for a free Ho^{3+} ion.

The small intensity reflections form a second group corresponding to a ferrimagnetic structure with partial compensation of magnetic moments (see Fig. 9b). The magnetic unit cell is identical to the crystallographic one ($\boldsymbol{k}$ = [0,0,0]). The holmium magnetic moments within each Wyckoff site are coupled ferrimagnetically, namely:

- the Ho1 moments (8*p* site) have two components: 1.9(2) μ_B along the *a*-axis and 2.2(2) μ_B along the *c*-axis with the total value of 2.9(2) μ_B (the Ho1 moments are inclined at an angle of about 40° to the *c*-axis),
- the Ho2 and Ho3 (two 4*i* sites) as well as Ho4 (4*g* site) moments have only the c-axis component equal to 4.5(2), −0.8(2) and −2.2(2) μ_B, respectively,
- the Ho5 atoms have no contribution to the ferrimagnetic component of the magnetic structure, and thus their magnetic moments are fixed to zero in Table 4.

Thermal evolution of the diffraction pattern indicate that two contributions to the magnetic structure, the antiferro- (AFM) ($\boldsymbol{k}$ = [0,0,½]) and ferrimagnetic (FiM) ($\boldsymbol{k}$ = [0,0,0]) ones, have different temperature dependence. Fig. 8 shows the intensity vs. temperature plot for selected Bragg reflections taken as representatives of the antiferro- and ferrimagnetic contributions to the magnetic structure together with those related to the crystal structure. Due to reflection overlapping the respective sums of intensities are shown as indicated in the Fig. 8 legend. Intensities of the AFM-related reflections decrease monotonically with temperature and are found absent in the pattern taken at 11.7 K. The highest rate of decrease is found between 4.2 K and 9.7 K. The intensities of the FiM-related reflections show different behavior, they undergo a rapid increase in the temperature range from 4.2 K to 9.7 K, then remain almost constant up to 11.7 K and finally gradually decrease and reach zero in the vicinity of 20 K.

Presented data indicate a coexistence of the antiferro- and ferrimagnetic orderings within the majority of temperature range of the

Table 5
Interatomic distances (δ) and coordination numbers (CN) in the $Ho_{11}Pd_4In_9$ compound, accordingly to the crystallographic data of $Ho_{11}Pd_4In_9$ presented in Table 1. Standard deviations are smaller than 0.006 Å. All distances within the first coordination spheres are listed.

Atom/CN			δ [Å]	Atom/CN			δ [Å]
Ho1	Pd	2x	2.803	Ho5	In2	8x	3.168
	In2	2x	3.151		Ho2	2x	3.481
CN = 14	In1	2x	3.234	CN = 12	Ho5	2x	3.633
	In1	2x	3.345				
	Ho1	1x	3.454	Pd	Ho1	2x	2.803
	Ho2	1x	3.488		Ho4	2x	2.921
	Ho1	2x	3.633	CN = 9	Ho3	2x	2.938
	Ho4	1x	3.830		In2	1x	2.992
	Ho3	1x	3.851		In1	1x	3.044
					In3	1x	3.140
Ho2	In1	4x	3.239				
	In2	4x	3.366	In1	In1	1x	2.996
CN = 13	Ho5	1x	3.481		Pd	1x	3.044
	Ho1	2x	3.488	CN = 12	Ho1	2x	3.234
	Ho2	2x	3.633		Ho2	2x	3.239
					Ho3	2x	3.327
Ho3	Pd	4x	2.938		Ho1	2x	3.345
	In1	4x	3.327		In1	2x	3.633
CN = 16	In3	2x	3.351				
	Ho3	2x	3.633	In2	Pd	1x	2.992
	Ho1	2x	3.851		In2	1x	3.109
	Ho4	2x	3.978	CN = 12	Ho1	2x	3.151
					Ho5	2x	3.168
Ho4	Pd	4x	2.921		Ho4	2x	3.344
	In2	4x	3.344		Ho2	2x	3.366
CN = 16	In3	2x	3.345		In2	2x	3.633
	Ho4	2x	3.633				
	Ho1	2x	3.830	In3	Pd	4x	3.140
	Ho3	2x	3.978		Ho4	4x	3.345
				CN = 14	Ho3	4x	3.351
					In3	2x	3.633

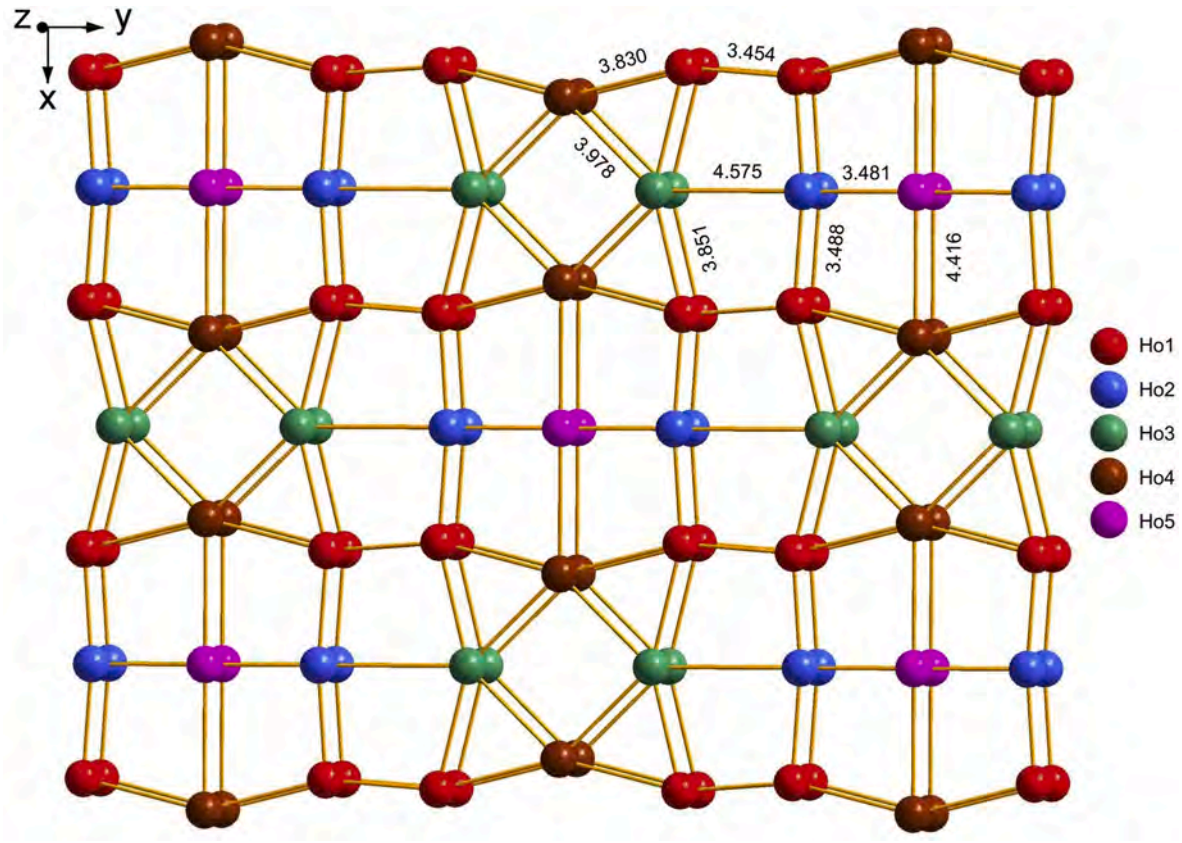

Fig. 10. The distributions of Ho atoms at different sites in $Ho_{11}Pd_4In_9$ and Ho–Ho interatomic distances in Å.

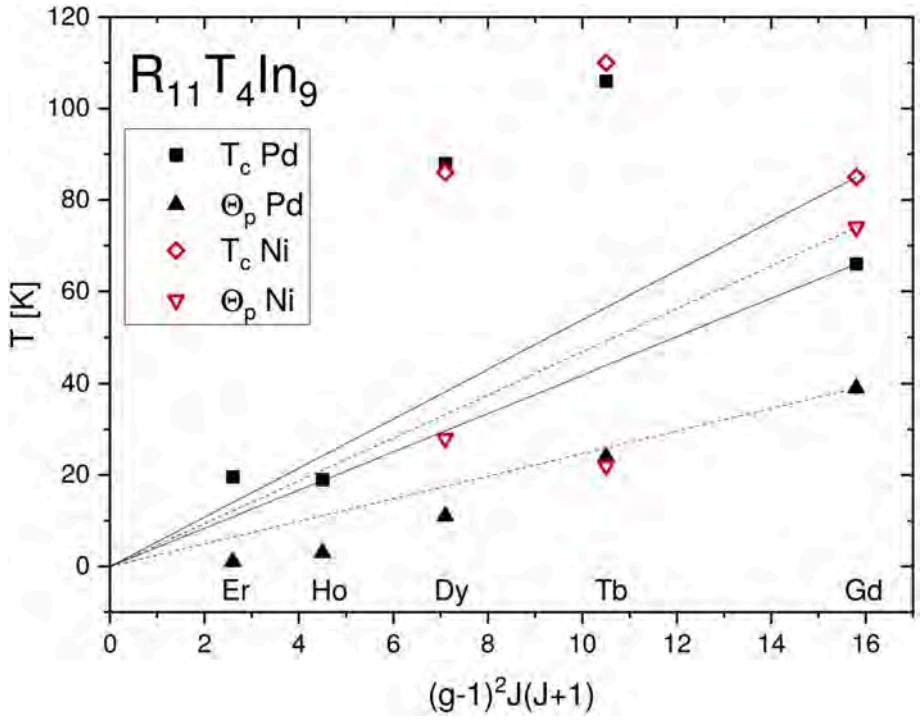

Fig. 11. The Curie temperatures (T_c) and paramagnetic Curie temperatures (θ_p) vs. de Gennes factor for $R_{11}T_4In_9$ (R = Gd–Er). The data for T = Ni are taken after Refs. [2,3] while for T = Pd are reported in this work. The straight lines indicate theoretical dependence, predicted by the RKKY theory, with Gd-based compounds taken as reference (see main text for details).

magnetically ordered state. The antiferromagnetic order is predominant at low temperatures while the ferrimagnetic one dominates at intermediate temperatures. Both magnetic phases disappear in the vicinity of the Curie temperature. The thermal evolution of different contributions to the magnetic structure is in agreement with the complex temperature dependence of magnetic susceptibility at low temperatures (see the inset in Fig. 4d).

4. Discussion

The work reports the results of X-ray and neutron powder diffraction and dc magnetic measurements for the $R_{11}Pd_4In_9$ (R = Y, Gd–Er) series of compounds. The X-ray diffraction data confirm the orthorhombic crystal structure of the $Nd_{11}Pd_4In_9$-type which was originally determined, using single-crystal X-ray diffractometry, for $Nd_{11}Pd_4In_9$ [8] and $Gd_{11}Ni_4In_9$ [4] and described in detail in Refs. [4,5,7,8,10]. The main determined structural features of the compounds are as follows: 1) the structure consists of two layers alternating along the shortest *c*-axis (much shorter than both the *a*- or *b*-axis), thus the layer of larger R atoms forms nets of tetragons and triangles at $z = 0$, while the layer of smaller in size (Ni,Pd)/In atoms forms nets of tetragons and pentagons at $z = ½$; 2) the crystal structure is formed by the AlB_2 (RNi_2) and CsCl (RIn)-type fragments; 3) the lattice parameters decrease linearly with decreasing effective ionic radius of rare earth (Fig. 3a) due to the lanthanide contraction; 4) polycrystalline samples of the compounds are built from well-defined fibers (or rods) quickly growing along the short *c*-axis due to the presence of short In–In chemical bonds in the *a*–*b* plane. The anisotropy of the crystal structure corresponds with strong anisotropy of the physical properties [5].

The refined lattice parameters and atomic coordinates, presented in Table 1, are in good agreement with the previous results for polycrystalline samples reported in Refs. [7] as well as with the single-crystal data for $Gd_{11}Ni_4In_9$ [4]. The lattice parameters of the $R_{11}Pd_4In_9$ compounds are only little larger than those for the isostructural $R_{11}Ni_4In_9$ intermetallics (see Fig. 3b) leading to similar magnetic properties in these two series of compounds. It is worth noting that the relative changes in the *a* and *b* lattice parameters ($\Delta a = [(a(Pd)\text{-}a(Ni))/a(Ni)] \times 100\%$, etc.), and accordingly the unit cell volume *V*, increase with decreasing effective ionic radius of the rare-earth element while the change in the shortest *c*-parameter rather decreases indicating a significant role of the transition element in the interatomic bonding. The refined interatomic distances and coordination numbers of atoms in $Ho_{11}Pd_4In_9$, listed in Table 5, well agree with the single-crystal data for $Gd_{11}Ni_4In_9$ [4].

The work reports the interesting magnetic properties of the $R_{11}Pd_4In_9$ compounds (R = Y, Gd–Er). $Y_{11}Pd_4In_9$ is a Pauli paramagnet while the other compounds (R = Gd–Er) order magnetically at low temperatures. The results of the macroscopic magnetic measurements are summarized in Table 2. The effective magnetic moments determined from high temperature data in the paramagnetic state are very close to the free R^{3+} ion values confirming that magnetic moments in $R_{11}Pd_4In_9$ (R = Gd–Er) are localized solely on the rare earth R^{3+} ions. The determined values of the paramagnetic Curie temperatures (θ_p) are positive indicating predominantly ferromagnetic character of the magnetic interactions. Noticeable deviations of the inverse magnetic susceptibility from the Curie-Weiss behavior, visible above respective Curie temperatures, are characteristic of short-range magnetic order. Temperature dependence of the magnetic susceptibilities (see the upper insets in Fig. 4a–e) and magnetization curves (see Fig. 5a–f) indicate a change of magnetic order from the antiferromagnetic ground state at low temperatures, through ferrimagnetic at intermediate temperatures and finally to paramagnetic state. The critical temperatures of magnetic ordering (T_c) are larger than the corresponding paramagnetic Curie temperatures (θ_p), indicating a presence of an antiferromagnetic contribution to the predominant ferromagnetic interactions, as expected for the high-temperature ferrimagnetic (FiM) phase. The critical and coercivity fields, determined from the magnetization curves and hysteresis loops, show a significant increase while comparing those of $Gd_{11}Pd_4In_9$ (L = 0, purely S state) and $Tb_{11}Pd_4In_9$ (L > 0), confirming the influence of crystalline electric field on magnetic properties. Further increase of the number of 4f electrons of the rare earth element leads to decrease of both the critical and coercivity fields.

The results of neutron diffraction experiment for $Ho_{11}Pd_4In_9$ show a presence of the complex temperature dependent magnetic structure at low temperatures. The holmium magnetic moments occupying five different Wyckoff sites are of different magnitudes (or are zero in the case of Ho5 in the FiM structure). The moments are parallel or antiparallel to the *c*-axis with exception for Ho1 in the FiM phase, whose moments are inclined at an angle of about 40° to the c-axis. Such a complex magnetic structure results from the complex crystal structure in which the rare earth atoms R occupy five nonequivalent sites with the similar R-R nearest neighbour interatomic distances within particular site or between the sites. The different rare earth sites are characterized by different local site symmetry, namely: m for the 8*p* site, m2m for the 4*i* sites, 2mm for the 4*g* site and mmm for the 2*a* site. Therefore, the magnetic structure results from competition between exchange interactions and local crystalline electric field.

The most of the Ho magnetic moments in the determined magnetic structures of $Ho_{11}Pd_4In_9$ (AFM and FiM) are parallel to the *c*-axis. This result is in agreement with the data for $R_{11}Ni_4In_9$ (R = Tb, Dy) where the *c*-axis was found to be an easy magnetization direction [5]. The magnetic structures in the isostructural $R_{11}Ni_4In_9$ (R = Tb, Ho) are complex with a number of temperature induced magnetic transitions and magnetic moments pointing at different directions [6], however, those structures are not the same as the ones reported here for $Ho_{11}Pd_4In_9$.

One can expect that such a scenario with a number of temperature- or field-induced magnetic transitions appearing consecutively is probably also realized in other members of the investigated $R_{11}Pd_4In_9$ (R = Gd–Er) family of compounds, whose magnetic structures have not yet been resolved.

Fig. 10 shows the distributions of the Ho atoms located at different sites. The shortest Ho–Ho distances are marked. In the majority of cases these distances are larger than the sum of atomic radii equal to 3.54 Å. Such a large R-R interatomic distances, found in both series of the $R_{11}T_4In_9$ (R = Ni, Pd) isostructural compounds, suggest that the magnetic interactions between the rare earth magnetic moments are predominantly driven by the indirect exchange interactions of the RKKY-type [13]. Fig. 11 shows the experimentally determined Curie temperatures and paramagnetic Curie temperatures plotted against the de Gennes factor. The straight lines indicate theoretical dependence, predicted by the RKKY theory, with Gd-based compounds taken as reference owing to the fact that the Gd^{3+} ion is in the S-state with zero orbital momentum and thus is not influenced by the crystalline electric field. The observed large discrepancy between the experimental and calculated temperatures, especially visible in T_C for R = Tb and Dy, indicates strong influence of the crystalline electric field (CEF) on stability of the magnetic order in both series of compounds [14]. Similar discrepancies, attributed to the influence of CEF, have been observed in RRh_4B_4 [15] and R_2CoGa_8 (R = rare earth element) [16].

Comparison of the magnetic data for both series of the isostructural $R_{11}T_4In_9$ (T = Ni, Pd) compounds indicates limited influence of the transition element T: Ni (3d) and Pd (4d). For both the series the magnetic moments are localized solely on the rare earth atoms. The Ni and Pd atoms do not possess localized magnetic moments. The compounds with R = Gd, Tb, Dy and T = Ni, Pd as well as two members of the Pd-series, namely, $R_{11}Pd_4In_9$ (R = Ho, Er), show similar magnetic properties at low temperatures. With increase of temperature the antiferromagnetic ground state transforms in to the ferrimagnetic structure at T_t which finally undergoes a transition to the paramegnetic state at T_c. The transition temperatures T_t and T_c are similar in both the series (see Table 1 in Ref. [3] and Table 2 in this work). $Ho_{11}Ni_4In_9$ is an exception as it is found purely antiferromagnetic while $Er_{11}Ni_4In_9$ is non-existent.

5. Summary

The $R_{11}Pd_4In_9$ compounds (R = Gd–Er) with the complex crystal structure in which the rare earth atoms occupy five nonequivalent sites present interesting magnetic properties. The magnetic moments, localized solely on the rare earth atoms, show complex magnetic ordering with the antiferromagnetic ground state at low temperatures. Applying temperature or external magnetic field induces a transition to the ferrimagnetic order. The critical temperature of magnetic order T_c, particularly those for R = Tb and Dy, do not obey the de Gennes relation indicating an influence of the crystalline electric field. The powder neutron diffraction data for $Ho_{11}Pd_4In_9$ show presence of two magnetic structures, namely: the antiferromagnetic ground state related to the propagation vector $\boldsymbol{k}$ = [0,0,½], dominant at low temperatures, and the ferrimagnetic phase with $\boldsymbol{k}$ = [0,0,0] dominant at intermediate temperatures. The Ho magnetic moments located at different Wyckoff sites are of different magnitudes and point at different directions indicating a strong influence of the crystalline electric field on formation of the magnetic state.

Declaration of competing interest

The authors declare that they have no known competing financial interests or personal relationships that could have appeared to influence the work reported in this paper.

CRediT authorship contribution statement

S. Baran: Formal analysis, Investigation, Writing - original draft, Writing - review & editing, Visualization. **Yu. Tyvanchuk:** Formal analysis, Investigation, Writing - original draft, Visualization. **B. Penc:** Formal analysis, Visualization. **Ya. Kalychak:** Writing - original draft. **A. Hoser:** Investigation. **A. Szytuła:** Investigation, Writing - original draft, Writing - review & editing.

Acknowledgements

The research was partially carried out with the equipment purchased thanks to the financial support of the European Regional Development Fund in the framework of the Polish Innovation Economy Operational Program (contract no. POIG.02.01.00-12-023/08).

References

[1] Ya Kalychak, V. Zaremba, R. Pöttgen, M. Lukachuk, R.-D. Hoffmann, Rare earth – transition metal – indides, ch. 218, in: K.A. Gschneidner Jr., J.-C.G. Bünzli, V. K. Pecharsky (Eds.), Handbook on the Physics and Chemistry of Rare Earths, 34Elsevier, Amsterdam, 2004, pp. 1–133, 2005.

[2] Yu. Tyvanchuk, S. Baran, R. Duraj, Ya. M. Kalychak, J. Przewoźnik, A. Szytuła, Crystal structure and magnetic properties of $Dy_{11}Ni_4In_9$, J. Alloys Compd. 587 (2014) 573–577, https://doi.org/10.1016/j.jallcom.2013.10.084.

[3] A. Szytuła, S. Baran, J. Przewoźnik, Yu Tyvanchuk, Ya Kalychak, Magnetic properties and specific heat data of $R_{11}Ni_4In_9$ (R = Pr, Nd, Sm, Gd and Tb) compounds, J. Alloys Compd. 601 (2014) 238–244, https://doi.org/10.1016/j.jallcom.2014.02.183.

[4] A. Provino, P. Manfrinetti, K.A. Gschneidner Jr., S.K. Dhar, D.L. Schlagel, T. A. Lograsso, G.J. Miller, S. Thimmaiah, H. Wang, A.M. Russell, A. Becker, Ya Mudryk, Self–assembled nano– to micron–size fibers from molten $R_{11}Ni_4In_9$ intermetallics, Acta Mater. 73 (2014) 27–36, https://doi.org/10.1016/j.actamat.2014.03.061.

[5] A. Provino, K.A. Gschneidner Jr., S.K. Dhar, C. Ferdeghini, Y. Mudryk, P. Manfrinetti, D. Paudyal, V.K. Pecharsky, The nano-microfibrous $R_{11}Ni_4In_9$ intermetallics: new compounds and extraordinary anisotropy in $Tb_{11}Ni_4In_9$ and $Dy_{11}Ni_4In_9$, Acta Mater. 91 (2015) 128–140, https://doi.org/10.1016/j.actamat.2015.03.003.

[6] C. Ritter, A. Provino, P. Manfrinetti, V.K. Pecharsky, K.A. Gschneidner Jr., S. K. Dhar, Magnetic structures of $R_5Ni_2In_4$ and $R_{11}Ni_4In_9$ (R = Tb and Ho): strong hierarchy in the temperature dependence of the magnetic ordering in the multiple rare-earth sublattices, J. Phys. Condens. Matter 27 (2015) 476001, https://doi.org/10.1088/0953-8984/27/47/476001.

[7] L. Sojka, M. Demchyna, B. Belan, M. Manyako, Ya Kalychak, New compounds with $Nd_{11}Pd_4In_9$ structure type in the systems RE-Pd-In (RE = La, Ce, Pr, Nd, Sm, Gd, Tb, Dy), Intermetallics 49 (2014) 14–17, https://doi.org/10.1016/j.intermet.2014.01.003.

[8] L. Sojka, M. Manyako, R. Černý, M. Ivanyk, B. Belan, R. Gladyshevskii, Ya Kalychak, $Nd_{11}Pd_4In_9$ compound – a new member of the homological series based on AlB_2 and CsCl types, Intermetallics 16 (2008) 625–628, https://doi.org/10.1016/j.intermet.2008.01.001.

[9] D. Das, D. Kaczorowski, Ferromagnetic Kondo lattice behavior in $Ce_{11}Pd_4In_9$, J. Magn. Magn Mater. 471 (2019) 315–320, https://doi.org/10.1016/j.jmmm.2018.09.104.

[10] M. Pustovoychenko, Yu Tyvanchuk, I. Hayduk, Ya Kalychak, Crystal structure of the $RE_{11}Ni_4In_9$ compounds (RE = La, Ce, Pr, Nd, Sm, Gd, Tb and Y), Intermetallics 18 (2010) 929–932, https://doi.org/10.1016/j.intermet.2010.01.003.

[11] J. Rodríguez–Carvajal, Recent advances in magnetic structure determination by neutron powder diffraction, Phys. B Condens. Matter 192 (1993) 55–69, https://doi.org/10.1016/0921-4526(93)90108-I. Commission on Powder Diffraction (IUCr), Newsletter 26 (2001) 12–19; J. Rodríguez–Carvajal,.

[12] R.D. Shannon, Revised effective ionic radii and systematic studies of interatomic distances in halides and chalcogenides, Acta Crystallogr. A 32 (1976) 751–767, https://doi.org/10.1107/S0567739476001551.

[13] P.G. de Gennes, Interactions indirectes entre couches 4f dans les métaux de terres rares, J. Phys. Radium 23 (1962) 510–521, https://doi.org/10.1051/jphysrad:01962002308-9051001.

[14] D.R. Noakes, G.K. Shenoy, The effect of a crystalline electric field on the magnetic transition temperatures of rare-earth rhodium borides, Phys. Lett. A91 (1982) 35–36, https://doi.org/10.1016/0375-9601(82)90258-4.

[15] B.D. Dunlap, L.N. Hall, F. Behroozi, G.W. Crabtree, D.G. Niarchos, Crystal-field effects and the magnetic properties of rare-earth rhodium borides, Phys. Rev. B 29 (1984) 6244–6251, https://doi.org/10.1103/PhysRevB.29.6244.

[16] D.A. Joshi, R. Nagalakshmi, S.K. Dhar, A. Thamizhavel, Anisotropic magnetization studies of R_2CoGa_8 single crystals (R = Gd, Tb, Dy, Ho, Er, Tm, Y, and Lu), Phys. Rev. B 77 (2008) 174420, https://doi.org/10.1103/PhysRevB.77.174420.